

Mutational analyses of HAMP helices suggest a dynamic bundle model of input–output signalling in chemoreceptors

Qin Zhou, Peter Ames and John S. Parkinson*

Biology Department, University of Utah, Salt Lake City, UT 84112, USA.

Summary

To test the gearbox model of HAMP signalling in the *Escherichia coli* serine receptor, Tsr, we generated a series of amino acid replacements at each residue of the AS1 and AS2 helices. The residues most critical for Tsr function defined hydrophobic packing faces consistent with a four-helix bundle. Suppression patterns of helix lesions conformed to the predicted packing layers in the bundle. Although the properties and patterns of most AS1 and AS2 lesions were consistent with both proposed gearbox structures, some mutational features specifically indicate the functional importance of an *x-da* bundle over an alternative *a-d* bundle. These genetic data suggest that HAMP signalling could simply involve changes in the stability of its *x-da* bundle. We propose that Tsr HAMP controls output signals by modulating destabilizing phase clashes between the AS2 helices and the adjoining kinase control helices. Our model further proposes that chemoeffectors regulate HAMP bundle stability through a control cable connection between the transmembrane segments and AS1 helices. Attractant stimuli, which cause inward piston displacements in chemoreceptors, should reduce cable tension, thereby stabilizing the HAMP bundle. This study shows how transmembrane signalling and HAMP input–output control could occur without the helix rotations central to the gearbox model.

Introduction

Many transmembrane signalling proteins in prokaryotes contain a 50-residue HAMP motif, so called because it occurs in histidine kinases, adenylyl cyclases, methyl-accepting chemotaxis proteins (MCPs) and certain phosphatases. HAMP sequences have few conserved

amino acid residues, but characteristic secondary structure features: two amphiphilic helices (AS1, AS2) joined by a non-helical connector (CTR) (Butler and Falke, 1998; Aravind and Ponting, 1999; Williams and Stewart, 1999). In transmembrane signalling proteins, the HAMP domain typically lies near the inner face of the cytoplasmic membrane, between the periplasmic sensing and cytoplasmic signalling portions of the molecule, where it plays a central role in converting stimulus-induced conformational changes into behaviour-controlling output signals (see Hazelbauer *et al.*, 2008 for a chemoreceptor review).

Chemoreceptors of the MCP family provide a tractable system for investigating the mechanism of HAMP-mediated input–output control. Native MCP molecules are homodimers of ~550 residue subunits organized into three functional modules (Fig. 1A): a transmembrane sensing module composed of a periplasmic ligand binding domain and four transmembrane helices, a signal-converting HAMP domain that adjoins one of the transmembrane helices in each subunit, and a four-helix bundle kinase control module connected to the HAMP domain. The kinase control portion of MCP molecules is highly conserved in sequence (Alexander and Zhulin, 2007) and tertiary structure (Kim *et al.*, 1999; Park *et al.*, 2006; Pollard *et al.*, 2009) and regulates the autophosphorylation activity of the histidine kinase, CheA. The kinase control module typically contains: four to six glutamic acid residues that are sites for adaptational modification (methylation and demethylation); a flexible bundle segment with a glycine hinge; and a hairpin tip that interacts with other MCP molecules, with CheA, and with CheW, a protein that couples CheA to receptor control.

Escherichia coli has two amino acid-sensing MCPs Tar (aspartate) and Tsr (serine) that have been extensively studied (Hazelbauer *et al.*, 2008). Both receptors contain two symmetric, negatively cooperative ligand binding sites at the dimer interface (Lee *et al.*, 1988; Milburn *et al.*, 1991; Biemann and Koshland, 1994; Lin *et al.*, 1994). In the unbound state, Tar and Tsr activate their associated CheA molecules (the kinase-on state). Binding of one attractant molecule produces an inward displacement of one of the transmembrane segments adjoining the HAMP domain (Falke and Hazelbauer, 2001). HAMP converts

Accepted 21 July, 2009. *For correspondence. E-mail parkinson@biology.utah.edu; Tel. (+1) 801 581 7639; Fax (+1) 801 581 4668.

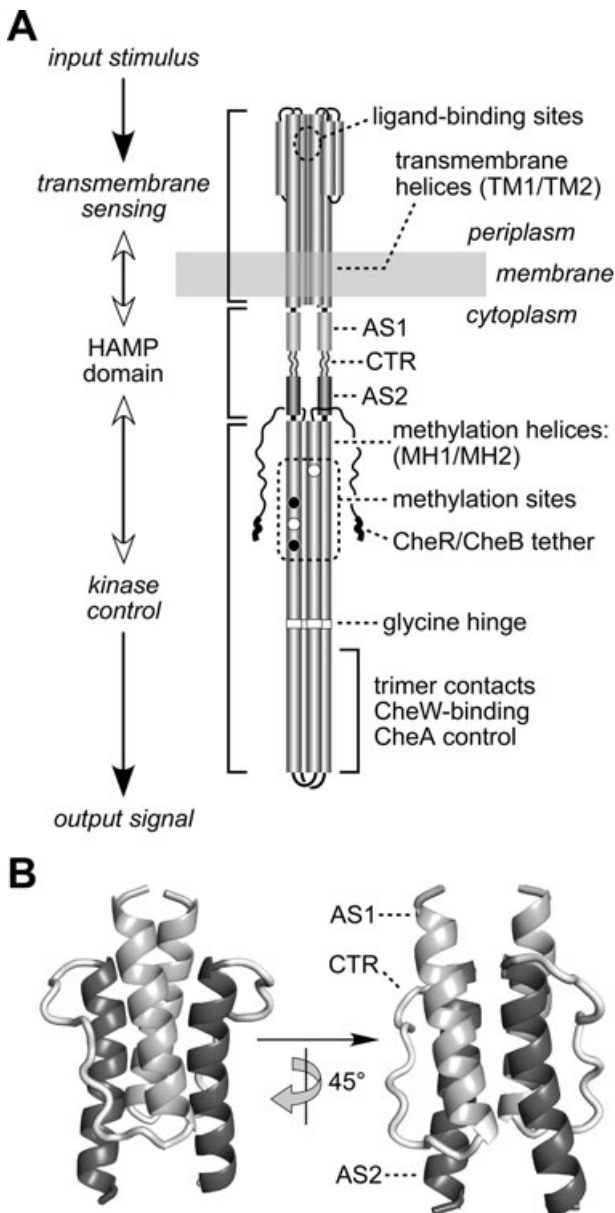


Fig. 1. Functional architecture of MCP molecules. **A.** Schematic model of the Tsr homodimer. The CheR/CheB tether (NWETF pentapeptide) marks the C-terminus of each subunit. Helical segments are represented as thickened cylinders, whose relative lengths are approximately to scale. Each Tsr subunit has two transmembrane helices (TM1, TM2) and two methylation helices (MH1, MH2) containing four principal methylation sites; two (black circles) are synthesized as glutamines and subsequently deamidated to glutamates (white circles). **B.** Modelled structure of the Tsr-HAMP domain. Atomic co-ordinates were obtained by threading the Tsr-HAMP sequence onto the Af1503 HAMP structure (Hulko *et al.*, 2006). The AS1 helix is labelled at its N-terminus; the AS2 helix is labelled at its C-terminus; CTR is the connector segment joining the two helices.

this piston-like movement into a conformational change of the kinase control region that deactivates CheA to elicit an appropriate chemotactic response. Locomotor behaviour and CheA activity are subsequently reset to prestimulus values by a sensory adaptation system that adjusts the detection sensitivity and dynamic range of the MCPs through reversible, feedback-controlled covalent modifications. Methylation or demethylation of the adaptation sites interposed between HAMP and the kinase control region influences both kinase activity and positioning of the signalling transmembrane helix, demonstrating bidirectional conformational control through HAMP (Lai *et al.*, 2006).

A recently determined nuclear magnetic resonance structure for an isolated HAMP domain from Af1503, a thermophile protein of unknown function, revealed a dimeric, parallel four-helix bundle, with the connector segments encircling helices from the same subunit (Hulko *et al.*, 2006) (Fig. 1B). The amino acid sequences of MCP HAMP domains readily thread onto the Af1503 HAMP structure and MCP HAMP domains exhibit structural features consistent with the Af1503 bundle (Swain and Falke, 2007; Ames *et al.*, 2008; Doebber *et al.*, 2008; Watts *et al.*, 2008). However, the nature of HAMP signalling states and their role in input–output signalling are still poorly understood. The report of the Af1503 HAMP structure also presented a two-state working model for HAMP, dubbed the gearbox model, in which the kinase-on and kinase-off output states corresponded to alternative HAMP bundle structures, interconvertible by concerted 26° counter-rotations of the HAMP helices (Hulko *et al.*, 2006). To date, there has been little published evidence for or against the gearbox model.

To explore the *in vivo* structure and function of a HAMP domain in a canonical chemoreceptor, and to experimentally address the gearbox model, we surveyed each residue in the AS1 and AS2 helices of Tsr to determine: (i) whether functionally critical residues corresponded to those predicted to participate in structure-stabilizing packing interactions in the four-helix HAMP bundle, (ii) whether function-disrupting lesions could be suppressed by compensatory structural changes in predicted partner helix residues and (iii) whether the patterns of mutations and suppression effects were consistent with the gearbox model. Our findings indicate that the Tsr-HAMP domain has a functionally important *in vivo* structure that closely resembles the four-helix bundle of Af1503 HAMP. However, that bundle may be the only functionally important Tsr-HAMP structure; our genetic evidence provided no strong support for the alternative bundle structure proposed in the gearbox model. Accordingly, we propose that HAMP signalling could simply involve modulated stability changes in the HAMP bundle. To stimulate further work in the field, we present possible mechanisms for the control

interactions between Tsr HAMP and its adjoining input and output domains.

Results

Mutational scan of the Tsr-HAMP helices

To identify the AS1 and AS2 residues most critical for Tsr function *in vivo*, we carried out a codon-by-codon mutagenesis of the *tsr* regions encoding residues K215-A233 (encompassing AS1) and E248-R265 (encompassing AS2) in two regulatable *tsr* expression plasmids, pRR53 and pPA114 (Fig. 2A). At optimal inducer concentrations [100 μ M isopropyl- β -D-thiogalactopyranoside (IPTG) or 0.6 μ M sodium salicylate respectively], pRR53 and pPA114 confer wild-type Tsr function to UU1250, a receptorless host strain carrying deletions of all five *E. coli* MCP family genes (*tsr*, *tar*, *tap*, *trg*, *aer*). Candidate mutant plasmids were tested in strain UU1250 for Tsr function at optimal induction conditions on tryptone soft agar plates. On the basis of these initial chemotaxis tests, each mutant plasmid was assigned to one of three functional categories: Tsr⁺ (colony size and morphology very similar to wild-type); Tsr[±] (reduced colony size and/or mutant ring morphology; see examples in Fig. 2B); and Tsr⁻ (complete loss of function, comparable to the vector control phenotype; see boxed examples in Fig. 2B).

We obtained about 13 mutant amino acids at each of the residues surveyed, sufficient to identify functionally critical helix residues and their important side-chain char-

acteristics (Fig. 3). We define important residues as those at which a majority of amino acid replacements demonstrably impaired Tsr function. Among those, we consider particularly critical residues to be the ones at which a majority of the deleterious replacements produced a complete loss-of-function (null) phenotype. By these criteria, AS1 has one important (P221) and six critical (L218, M222, L225, I229, I232, A233) residues; AS2 has six critical residues (E248, M249, L252, L256, M259, L263) (Fig. 3A).

Residues P221 (AS1) and E248 (AS2) are conserved, defining features of HAMP domains (Aravind and Ponting, 1999; Williams and Stewart, 1999). We generated additional mutations at these two positions by site-directed mutagenesis to obtain a complete set of amino acid replacements for each. Despite its presence in nearly every HAMP domain, P221 is not a highly critical residue in Tsr-HAMP, although most replacements at this position did impair Tsr function to some extent (Fig. 3A). E248 proved much less tolerant of amino acid replacements. Only cysteine and aspartate preserved wild-type function, whereas most other E248 replacement mutants exhibited a null phenotype (Fig. 3A).

We also made site-directed mutations at some HAMP codons to obtain proline replacements at every AS1 and AS2 residue. AS2 was quite sensitive to proline replacements; nearly all positions yielded a null defect (17/18 Tsr⁻; Fig. 3A), consistent with the premise that this HAMP segment has helical character *in vivo*. AS1 also proved sensitive to proline replacements, but replacements at some AS1 residues did not cause a complete loss of function (11/18 Tsr⁻; 6/18 Tsr[±]). We note that four of the six partially functional AS1 proline mutants had replacements close to P221, the naturally occurring AS1 proline that is optimal for HAMP function (see above). We conclude that AS1 also has helical character *in vivo*, but its structural stability may be less critical to HAMP function than that of AS2.

In all, we characterized 51 AS1 and 80 AS2 missense mutants with complete loss-of-function Tsr phenotypes. The remainder of this report deals exclusively with these Tsr-HAMP⁺ null mutants.

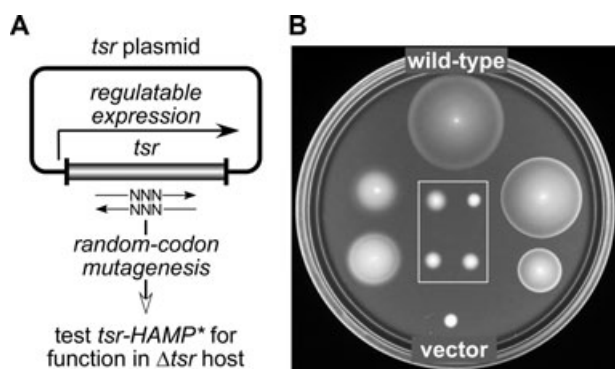


Fig. 2. Isolation of Tsr-HAMP mutants.

A. Strategy for constructing mutations. Mutations were created by randomizing the sequences of individual HAMP codons in plasmids carrying the *tsr* coding region under inducible expression control. Candidate plasmids were tested for Tsr function in UU1250, a receptorless host that lacks *tsr* and other MCP family receptors.

B. Examples of mutant Tsr-HAMP phenotypes. UU1250 transformants from (A) were tested for Tsr function on tryptone soft agar plates containing 12.5 μ g ml⁻¹ chloramphenicol and 0.6 μ M sodium salicylate and incubated at 30°C for 7 h. The wild-type control was pPA114; the vector control was pKG116. Eight mutant examples are shown: the two on the left (I229Y, M249S) and the two on the right (I226M, S255E) exhibit reduced or impaired Tsr function (i.e. Tsr[±]). The four boxed mutants have null defects (i.e. Tsr⁻).

Critical AS1 and AS2 residues correspond to packing faces in the HAMP four-helix bundle

The Af1503 HAMP structure exhibits 'complementary *x-da*' helix packing interactions in which three residue positions along the hydrophobic face of each helix contribute to the stability of the four-helix bundle (Hulko *et al.*, 2006) (Fig. 3B). Note that the residue designations in the *x-da* arrangement differ from those in the *a-d* heptad repeat in many coiled coils. To identify corresponding residues in the two packing arrangements (in Figs 3 and

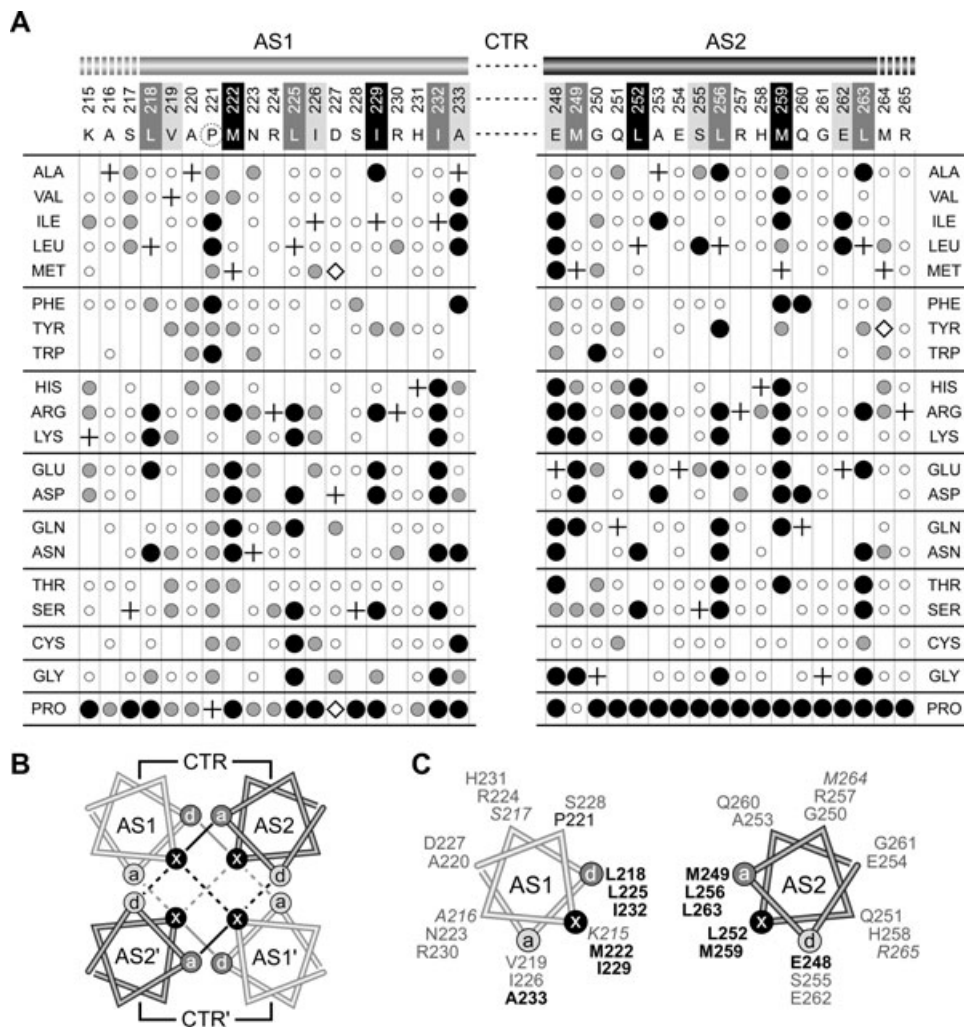


Fig. 3. Mutant phenotypes and packing faces of AS1 and AS2 helices in Tsr HAMP.

A. AS1 and AS2 missense mutants. Residue numbers and wild-type amino acids of Tsr HAMP are shown at the top of the figure. In the *x-da* packing notation, critical *d* positions in AS1 and critical *a* positions in AS2 are shaded dark grey. Non-critical *a* positions in AS1 and non-critical *d* positions in AS2 are shaded light grey. Residues at *x* positions in both helices are shaded black. The dashed circle around P221 indicates that this residue is less critical, but also important for function. Missense changes obtained at each residue are indicated by circles below the corresponding wild-type residue: small, open circles = Tsr⁺; intermediate-sized grey circles = Tsr[±]; large black circles = Tsr⁻. Plus symbols indicate the wild-type residues at each position. Where no symbol is given, that particular replacement was not isolated. Mutants denoted by open diamonds expressed Tsr at less than 25% of the wild-type level; all other mutants expressed Tsr at 50% or more of the wild-type level (Table S1).

B. Helix packing in the *x-da* four-helix HAMP bundle. Helical wheels, viewed towards the C-terminus from the N-terminal side, show the *x*, *d* and *a* positions of the bundle-stabilizing residues (Hulko *et al.*, 2006). Two layers of hydrophobic packing interactions are indicated by black (upper layer) and grey (lower layer) lines. Interactions that stabilize the intrasubunit interface are indicated by solid lines; interactions that stabilize the intersubunit interface are indicated by dashed lines.

C. One subunit of the *x-da* bundle. The AS1 and AS2 residues important or critical (bold) for function are labelled in black type; non-critical residues are labelled in grey type. Italic labels indicate residues on the N-terminal (K215-S217) or C-terminal (M264-R265) side of the HAMP bundle that may serve as transmission links to adjacent domains (see Discussion).

7), positions critical to both arrangements are shown with black and dark grey shading and less critical 'edge' residues with light grey shading. In *x-da* packing, the side-chains of symmetry-related *x* residues face one another in 'knob-to-knob' orientation, whereas the side-chains of the flanking *d* and *a* residues lie one helical turn above or below and pack against the *x* residues in the other helix

(Fig. 3B). In this packing arrangement, some *a/d* residues (dark grey) contribute to intrasubunit interactions, whereas others (light grey) contribute to intersubunit interactions. Note, however, that the *x* residues stabilize both the intra- and intersubunit helix interfaces (Fig. 3B). In Tsr HAMP, all but one of the functionally critical residues in each helix fell at two packing positions (*x* and *d* in AS1

and *a* and *x* in AS2; see Fig. 3C), indicating that those two positions play predominant roles in stabilizing the Tsr-HAMP structure. These mutational features are consistent with a four-helix bundle structure for Tsr HAMP. If that bundle has an *x-da* arrangement, then the mutation patterns suggest that packing interactions within each subunit (involving the dark grey *a* and *d* positions in Fig. 3C) are more critical to function than are those at the interface between subunits (involving the light grey *a* and *d* positions in Fig. 3C).

Expression level and stability of Tsr-HAMP* proteins

Owing to their loss-of-function nature, we cannot be certain that Tsr-HAMP* null mutant proteins retain native or near-native structures. However, at optimal induction conditions for wild-type Tsr, all but three of the null mutants (D227M, D227P and M264Y) exhibited a steady-

state Tsr protein level above 50% of wild type (Fig. 3A; Table S1), which indicates that the vast majority of null mutant proteins have essentially wild-type intracellular stabilities, and perhaps mainly native structures, as well.

Dominance and asymmetry tests of Tsr-HAMP* lesions

To assess the extent of structural perturbation in Tsr-HAMP* null mutants, we tested their signalling properties in heterodimers that contained one wild-type (HAMP⁺) subunit. These tests were done by expressing plasmid-encoded Tsr-HAMP* subunits in *tsr* mutant hosts that had a recessive serine-binding defect (R69E or T156K) (Ames *et al.*, 2008). Tsr heterodimers containing either the R69E or T156K lesion in one subunit have one functional serine-binding site, but the subsequent piston displacement takes different routes (Fig. 4A). In R69E heterodimers, ligand-induced piston motions occur in the R69E subunit,

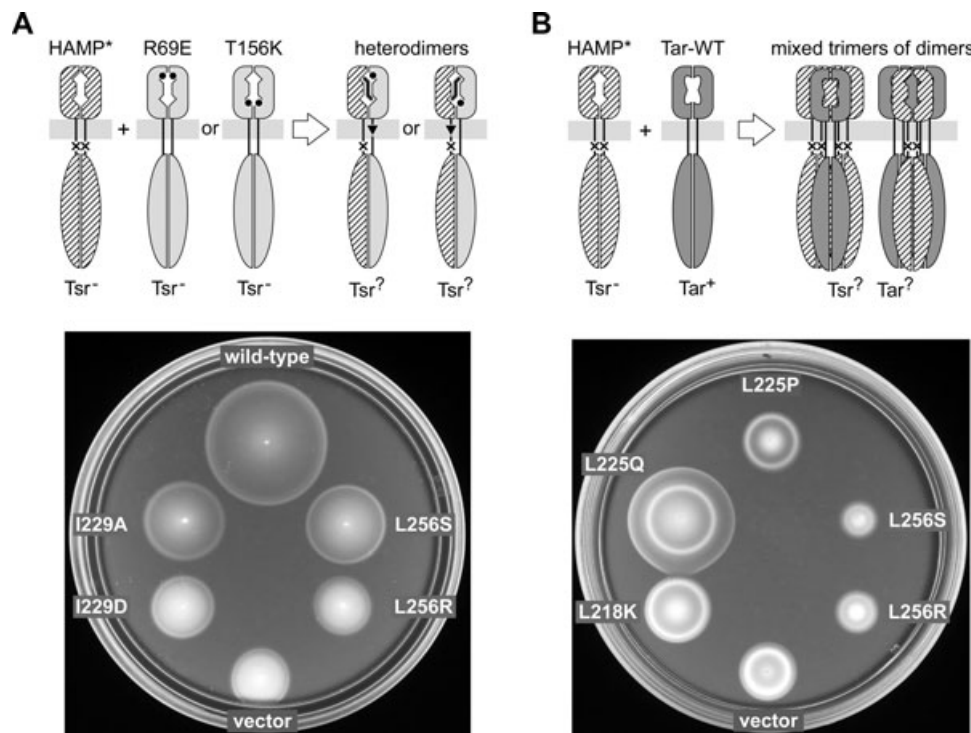


Fig. 4. Functional tests of Tsr-HAMP mutations.

A. Dominance and asymmetry test. Upper: plasmid-encoded mutant Tsr-HAMP (HAMP⁺) subunits were expressed in a host strain with chromosomally encoded Tsr-R69E or Tsr-T156K subunits, which have lesions at the serine-binding site. The resulting heterodimers have one functional binding site, which produces ligand-induced piston motions through the wild-type HAMP subunit (in the case of R69E) or through the mutant HAMP subunit (in the case of T156K). Lower: examples of dominant and recessive Tsr-HAMP defects. UU2378 (*tsr-T156K*) cells containing pPA114 derivatives were tested for Tsr function on tryptone soft agar plates containing 12.5 $\mu\text{g ml}^{-1}$ chloramphenicol and 0.6 μM sodium salicylate and incubated at 30°C for 7.5 h. The wild-type control was pPA114; the vector control was pKG116. Tsr-HAMP mutants I229A and L256S are recessive; I229D and L256R are dominant.

B. Jamming and rescue test. Upper: plasmid-encoded Tsr-HAMP* molecules were expressed in a *tar⁺ Δtsr* host strain. Tar and Tsr subunits do not form heterodimers, but do form mixed trimers of dimers, in which some Tsr defects regain function (rescue) and other Tsr defects spoil Tar function (jamming). Lower: examples of rescuable and jamming Tsr-HAMP defects. UU1623 cells containing pPA114 derivatives were tested for Tsr function on tryptone soft agar plates containing 12.5 $\mu\text{g ml}^{-1}$ chloramphenicol and 0.6 μM sodium salicylate and incubated at 32.5°C for 9 h. The vector control was pKG116. L256S and L256R jam Tar; L225Q is rescuable (and does not jam Tar); L218K and L225P are neither rescuable nor jamming.

whereas in T156K heterodimers, the piston displacement occurs in the opposite, HAMP* subunit (Yang *et al.*, 1993). Because the mutant homodimers cannot support Tsr function, positive tests identify recessive lesions and negative tests identify dominant lesions. We assume that recessive HAMP lesions have relatively modest structural changes, whereas dominant HAMP lesions must have more drastic structural changes that perturb HAMP structure even in association with a wild-type HAMP subunit. Examples of recessive and dominant Tsr-HAMP* behaviours are shown in Fig. 4A; test results for all Tsr-HAMP* nulls are summarized in Table S1 (and in Fig. 7C, to be discussed in more detail below). Of 128 Tsr-HAMP* null mutants tested, 30 had dominant defects; the remainder were recessive. However, none of the mutants exhibited functional asymmetry in these tests, for example, by blocking signal transmission in the T156K heterodimer, but not in the R69E heterodimer. The symmetric behaviour of all HAMP* null mutants in these tests implies that AS1 and AS2 lesions disrupt Tsr function by interfering with symmetric structural interactions between the two HAMP subunits in a Tsr dimer. Thus, these test results are also consistent with a four-helix bundle HAMP structure.

Rescue and jamming tests of Tsr-HAMP* lesions

To assess the extent of functional perturbation in Tsr-HAMP* null mutants, we tested their signalling properties in cells containing wild-type Tar molecules, the aspartate chemoreceptor. These tests were done by expressing plasmid-encoded Tsr-HAMP* subunits in a *tar*⁺, but otherwise receptorless, host and assessing its Tsr and Tar function on tryptone soft agar plates (Ames *et al.*, 2008). Tsr and Tar subunits do not form heterodimers (Milligan and Koshland, 1988), but Tsr and Tar homodimers can form mixed trimer of dimer signalling teams (Fig. 4B) (Ames *et al.*, 2002; Studdert and Par-

kinson, 2004; Ames and Parkinson, 2006). Some Tsr* defects are functionally rescued by wild-type Tar team partners, and other Tsr* defects can block or jam Tar function in the mixed teams. We assume that rescuable Tsr* mutants have relatively modest functional defects, whereas jamming Tsr* mutants have relatively severe defects that prevent team function, despite the presence of wild-type members. Examples of rescuable and jamming Tsr-HAMP* behaviours are shown in Fig. 4B; test results for all Tsr-HAMP* nulls are summarized in Table S1 (Jamming results are also summarized in Fig. 7C, to be discussed in more detail below). Among 128 null mutants, 24 exhibited jamming properties and 51 others had rescuable defects. Thus, at least 75/128 HAMP* null proteins most likely form mixed trimers of dimers with wild-type Tar molecules. We did not directly test the non-rescuable and non-jamming HAMP* mutants for trimer-of-dimer formation, but some of those mutant receptors are probably able to form mixed trimers with Tar, as well, even though they cannot influence the signalling properties of the mixed teams (Ames *et al.*, 2002; Ames and Parkinson, 2006; Mowery *et al.*, 2008).

Compensatory interactions between mutant AS1 and AS2 helices

The hydrophobic residues that stabilize the four-helix HAMP bundle interact in four packing layers (Hulko *et al.*, 2006) (Fig. 5A). In addition to intersubunit interactions between helix residues, within each subunit the *x* residues in one HAMP helix pack against residues at the *d* and *a* positions in the same layer of the other HAMP helix: M222 (*x*)/E248 (*d*)/M249 (*a*) [layer 1], L252 (*x*)/L225 (*d*)/I226 (*a*) [layer 2], I229 (*x*)/S255 (*d*)/L256 (*a*) [layer 3] and M259 (*x*)/I232 (*d*)/A233 (*a*) [layer 4] (Fig. 5A). These structural features suggest that deleterious amino acid replace-

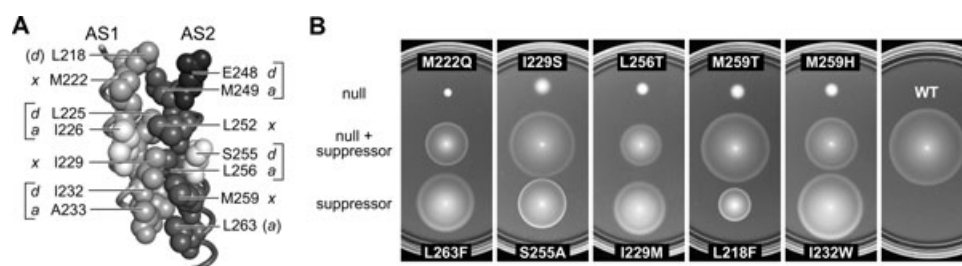


Fig. 5. Tsr-HAMP packing layers and example suppression pairs.

A. Side view of AS1-AS2 packing interactions in one subunit of the modelled four-helix Tsr-HAMP bundle. Space-filled residues compose the packing interface. Critical AS1 residues are shown with light grey atoms; critical AS2 residues with either dark grey or black (E248) atoms. Non-critical residues at the packing interface (I226, S255) have white atoms. Brackets denote the four packing layers (*x* in one helix; *a*, *d* in the other). L218 (*d*) and L263 (*a*) participate in packing interactions at the top and bottom of the bundle respectively.

B. Examples of suppression quality. Derivatives of pPA114 carrying a Tsr-HAMP null mutation alone, a suppressor mutation alone and the double mutant combination were tested for Tsr function in receptorless host strain UU1250. Transformant cells were placed on tryptone soft agar plates containing 12.5 µg ml⁻¹ chloramphenicol and 0.6 µM sodium salicylate and incubated at 30°C for 7 h.

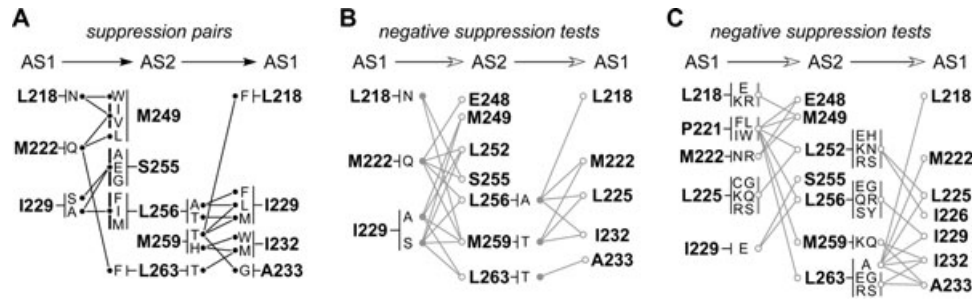


Fig. 6. Summary of AS1-AS2 suppression tests.

A. Positive suppression pairs. Horizontal arrows at the top point away from the helix with a starting null lesion and towards the targeted helix. Thick vertical lines next to some amino acid replacements at suppressor residues indicate several different changes that suppressed the same null defect.

B. Negative suppression tests involving suppressible null alleles. This diagram indicates targeted residues that did not give rise to suppressors of null defects known to be suppressible from the tests in (A). Not all combinations of null and target residues were tested. Grey circles indicate previously suppressible null alleles; open circles indicate targeted residues that yielded no suppressors.

C. Negative suppression tests of other null alleles. This diagram summarizes combinations of null defects and targeted residues that did not give rise to suppression effects. Not all combinations of null and target residues were tested. Thick vertical grey lines group multiple null lesions tested at some residues.

ments at a critical residue in one HAMP helix could act by destabilizing helix packing interactions. Accordingly, null defects in a HAMP helix might be suppressible by a compensatory change at a packing partner residue in the other HAMP helix. To test this possibility, we chose amino acid replacements in AS1 or AS2 that caused null phenotypes and scanned potential packing partner residues in the other helix for amino acid changes that could restore some degree of signalling function. To survey a full spectrum of amino acid replacements at potential packing partners, we targeted individual residues in each Tsr-HAMP null mutant for all-codon mutagenesis and tested pools of several hundred mutant plasmids for ones with enhanced Tsr function.

Nine Tsr-HAMP null lesions proved suppressible; examples are shown in Fig. 5B and summarized in Fig. 6A. All suppressible defects were recessive, most (7/9) were non-jamming and functionally rescuable (Fig. 6A and Table S1). These properties suggest that suppressible lesions have relatively modest structure- and function-perturbing character. The suppressible null defects had polar amino acid replacements at one of the critical hydrophobic residues (AS1: L218N, M222Q, I229A/S; AS2: L256A/T, M259H/T, L263T). Except for one residue (S255A/E/G), the suppressors involved replacements at other critical hydrophobic residues (AS2: M249I/L/V/W, L256F/I/M; L263F; AS1: L218F; I229F/L/M; I232M/W; A233G). However, contrary to our initial expectations, the suppressor changes at hydrophobic residues did not involve polar amino acid replacements, but rather hydrophobic ones, often with different side-chain volumes than the wild-type residue. This finding implies that relatively modest changes in HAMP packing interactions can overcome the destabilizing effects of polar replacements at critical helix residues.

Of the 18 different amino acid replacements found as suppressors (see Fig. 6A), we had obtained 14 of them in our HAMP mutagenesis study (Fig. 3A). Ten of these single-replacement mutants exhibited essentially wild-type Tsr function (see L263F, I229M, I232W in Fig. 5B), whereas the other four formed small, sharp-edged colonies on tryptone soft agar plates, indicating somewhat reduced Tsr function (see S255A and L218F in Fig. 5B). Interestingly, the mutations causing partial Tsr defects seemed to be the most effective suppressors, yielding large, wild-type colony phenotypes when combined with a suppressible null lesion (Fig. 5B).

To assess the residue position and side-chain specificity of these suppression effects, we tested the suppressible mutants, and other null defects at the same residues, in combination with a variety of target residues. Residue combinations that did not lead to a suppression effect are summarized in Fig. 6B and C. Most targeted residues failed to suppress the starting null defects. For example, although the M222Q null defect was suppressible by changes at M249 and L263 (Fig. 6A), it was not suppressible by replacements at E248, L252, S255, L256 or M259 (Fig. 6B). Similarly, the M259T null defect was suppressible by changes at L218, I229 and A233 (Fig. 6A), but not by any amino acid replacement at M222, L225 or I232 (Fig. 6B). Moreover, other null defects at these same residues (M222N, M222R; M259K, M259Q) were not suppressible by any amino acid changes at the targeted suppressor residues (Fig. 6C). In all, 112 combinations of null mutations and target residues were tested for suppression effects. Only 6/61 AS1 null combinations and 7/51 AS2 null combinations yielded suppressors. This high degree of residue and side-chain specificity is consistent with restoration of function through compensatory structural changes, presumably ones that interact to sta-

bilize the native HAMP structure. Most of the positive suppression pairs conformed to the packing layers of the *x-da* four-helix bundle (see Fig. 9A, to be discussed in more detail below), providing additional support for this HAMP structure in Tsr.

Discussion

The four-helix HAMP bundle

The structure of the Af1503 HAMP domain has provided important clues to the mechanism(s) of HAMP signalling (Hulko *et al.*, 2006). The Af1503 HAMP domain is dimeric, with the AS1 and AS2 helices of both subunits organized in a parallel four-helix bundle (Hulko *et al.*, 2006). Because chemoreceptors of the MCP family and other HAMP-containing proteins have a dimeric native structure, many HAMP domains could have a four-helix bundle structure. There is growing support for this idea. Cysteine-scanning (Butler and Falke, 1998) and disulphide-mapping (Swain and Falke, 2007) studies have provided *in vitro* evidence for a four-helix HAMP bundle in Tar, the aspartate chemoreceptor. Similar *in vivo* studies of Aer, an MCP-like aerosensor, have also indicated a four-helix bundle HAMP structure (Watts *et al.*, 2008). In HtrII, an MCP-like transducer that interacts with the sensory rhodopsin photoreceptor of *Natronomonas pharaonis*, HAMP signalling is accompanied by changes in the diffusion coefficients of AS1 and AS2 (Inoue *et al.*, 2008) and by conversion from a 'dynamic' state to a 'compact' structure (Doebber *et al.*, 2008). Both results are at least consistent with a four-helix bundle.

Our Tsr-HAMP suppression studies are also consistent with a four-helix bundle organization. The Af1503 HAMP bundle is stabilized by four layers of hydrophobic packing interactions (Hulko *et al.*, 2006). We tested this structural feature by identifying compensatory changes that could restore function to AS1 and AS2 mutants with null lesions at predicted packing residues (Fig. 9A). Most suppression effects occurred between residues in the same (5/10) or adjacent (3/10) packing layers. Moreover, two of the adjacent layer effects (L218/M249 and L263/I232) involved the bundle-capping residues (L218, L263), which could have special structural roles. The remaining two suppression effects (L218/M259 and M222/L263) occurred across multiple layers, but both of these long-range interactions involved the bundle-capping residues, as well. All suppression effects were highly specific with respect to both residue position and side-chain character, consistent with restoration of function via compensatory conformational changes. We conclude that the suppression analysis reflects structural interactions between the AS1 and AS2 helices that are consistent with a four-helix bundle.

Mutational evidence for an x-da packing arrangement in the Tsr-HAMP bundle

The experimentally determined Af1503 HAMP structure exhibits a 'complementary *x-da*' packing arrangement of the helices in the bundle (Hulko *et al.*, 2006). Hulko *et al.* (2006) suggested that a more conventional '*a-d*' packing arrangement could represent an alternative HAMP signalling conformation. The two bundle structures are related by a concerted 26° counter-rotation of each of the four helices, analogous to meshed gears in a transmission (the 'gearbox'; see Fig. 7A and B). In the *x-da* structure, three residue positions contribute to bundle stability (Fig. 7A). The *x* positions are structurally distinct from the flanking *a* and *d* positions; their side-chains project into the bundle core and interact with their counterparts in the opposing subunit (Fig. 7A). In contrast, the two critical hydrophobic positions in the *a-d* arrangement (dark grey shading in Fig. 7B) contribute more or less equally to bundle integrity. The *d* position in AS1 and the *a* position in AS2 correspond to critical *a* and *d* residues in the *x-da* arrangement (dark grey shading in Fig. 7A). However, in the *a-d* arrangement, the *a* positions in AS1 and the *d* positions in AS2 (black shading in Fig. 7B) correspond to *x* residues in the *x-da* arrangement (black shading in Fig. 7A). Note that the non-critical *a/d* positions in the *x-da* arrangement (light grey shading in Fig. 7A) correspond to *g* or *e* 'edge' residues in the *a-d* arrangement (light grey shading in Fig. 7B). It follows that in the *a-d* packing arrangement, *x* and *a/d* residues should have comparable mutational sensitivities, whereas in the *x-da* arrangement, they might have different mutational properties that reflect their different structural environments.

The dominance properties of proline and arginine replacements at critical AS1 residues are more consistent with an *x-da* bundle organization than with an alternative *a-d* arrangement. Arginine replacements at the AS1 *x* positions (black shading in Fig. 7C) caused dominant defects, whereas at the critical AS1 *d* positions (dark grey shading in Fig. 7C), arginine replacements caused recessive defects. The more severe structural consequences of arginine replacements at *x* positions are consistent with their core location in the *x-da* structure, which should not have enough space to accommodate a large, polar residue. In contrast, proline replacements were dominant at 2/3 critical AS1 *d* positions (L218, L225), but recessive at the two *x* positions in AS1 (Fig. 7C). These differences also distinguish the *x* and *d* residue positions in AS1. Perhaps prolines are better tolerated at *x* positions because of their relatively small volume and the fact that hydrophobicity may be less critical to bundle stability at fully buried positions (Hulko *et al.*, 2006). The most parsimonious conclusion to draw from this evidence is that

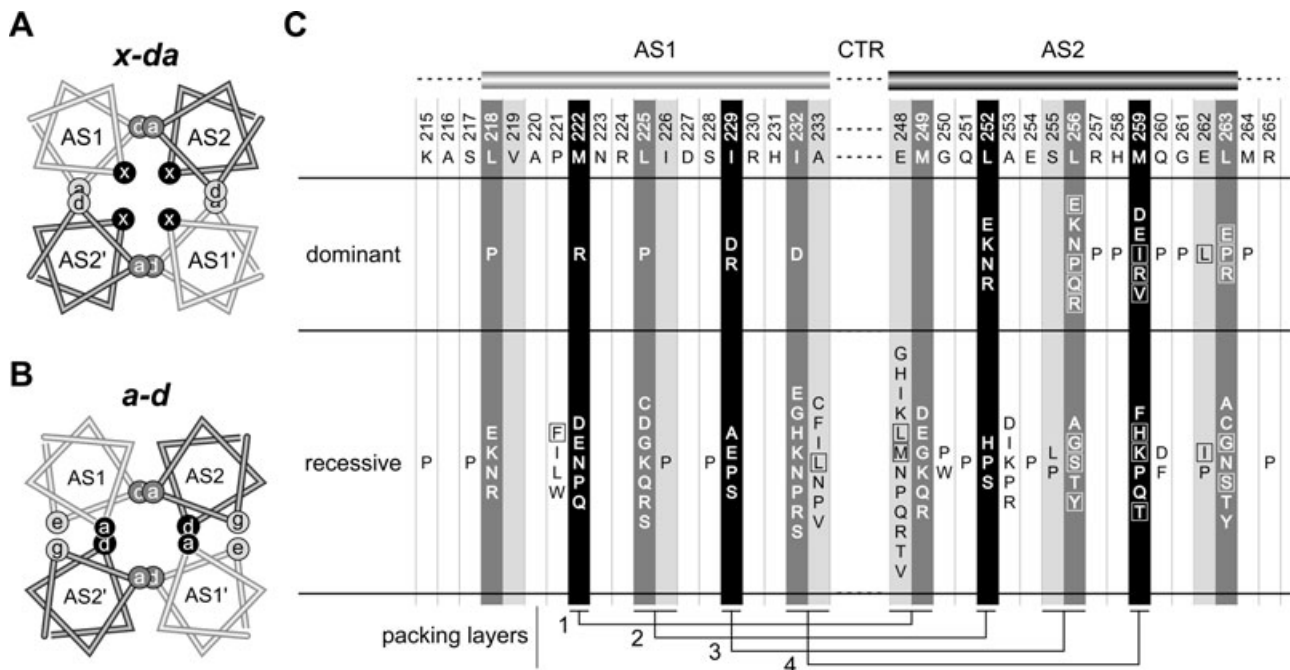


Fig. 7. Bundle arrangements and null lesions in the Tsr-HAMP AS1 and AS2 helices.

A. Helical wheel cross-section of the *x-da* packing arrangement. This view is similar to that shown in Fig. 3B, but the helices have been moved closer together and overlapped to emphasize the layers and packing interactions. Residues at overlapping *a* and *d* positions contribute to intrasubunit (dark grey) or intersubunit (light grey) packing interactions; residues at the *x* positions (black) stabilize both the intra- and intersubunit interface, as summarized in Figs 3B and 5A.

B. Helical wheel cross-section of a possible *a-d* bundle. This HAMP packing arrangement has not been observed experimentally, but was suggested to be the functional alternative to the *x-da* signalling state (Hulko *et al.*, 2006). Overlapping sites indicate packing layers and residue interactions. As in the *x-da* arrangement, interactions between dark grey *a/d* residue positions stabilize the intrasubunit interface. However, the black *a/d* residue positions that stabilize the intersubunit interface are *x* residues in the *x-da* arrangement of (A). The *e* (AS1) and *g* (AS2) positions (light grey shading) correspond to the non-critical *a* (AS1) and *d* (AS2) residues in the *x-da* arrangement.

C. Summary of null (Tsr) lesions in the AS1 and AS2 helices. Wild-type amino acids and residue numbers are given below the AS1 and AS2 cartoons. Shading of the residue positions corresponds to that of the *x*, *d* and *a* positions in the HAMP bundles of (A) and (B). Boxes enclose amino acid replacements that caused moderate to severe jamming behaviour (E2 or E3 classification, see Table S1). Residue interactions in the four packing layers are shown at the bottom of the figure.

the *x-da* packing arrangement is the only functionally important four-helix HAMP bundle in Tsr.

Control linkage between the HAMP and methylation bundles

The mutation patterns of Tsr-HAMP helices suggest that AS2 has a more central role than AS1 in HAMP signalling (Fig. 7C). (i) The preponderance of dominant (24/30) and jamming (22/24) mutations occurred in AS2, indicating that AS2 lesions have more drastic structural and functional consequences than do AS1 lesions, which were mostly recessive and non-jamming. (ii) Residues 256–264, spanning the C-terminal region of AS2, were also especially sensitive to proline replacements, with 7/11 replacements causing dominant defects. Nowhere else in HAMP did proline replacements at non-critical residue positions cause dominant behaviour (Fig. 7C). The heightened sensitivity to proline replacements probably

reflects the importance of helix strength at the AS2/MH1 junction.

The AS2 helices connect to the MH1/MH1' methylation helices of the kinase control domain, a long four-helix bundle of two interwound, anti-parallel coiled coils (Bass and Falke, 1999; Kim *et al.*, 1999; Park *et al.*, 2006; Alexander and Zhulin, 2007). Stimulus signals transmitted through HAMP impinge on the MH1 and MH1' segments to modulate output signals from the kinase control bundle. Conversely, the modification states of the methylation helices in the kinase control bundle impinge on HAMP to modulate the transmembrane helices and the stimulus-sensing portion of the receptor molecule (Lai *et al.*, 2006). The heptad phasing of the AS2 and MH1 helices is out of register by +4 (or –3) residues, a so-called 'stutter' (Brown *et al.*, 1996; Lupas, 1996) (compare the *a* heptad positions in AS2 and MH1 in Fig. 8A). Stutters destabilize coiled-coil pairing interactions, producing an underwound or kinked structure (Brown *et al.*, 1996; Lupas, 1996). The

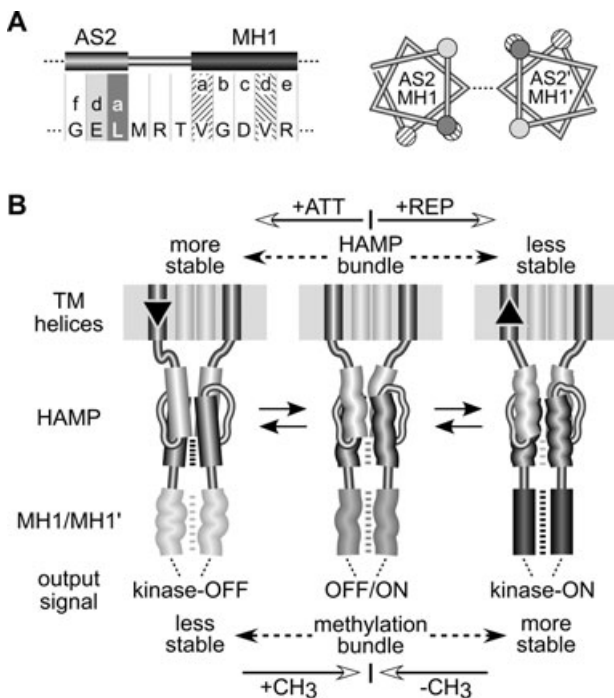


Fig. 8. Mechanistic model of HAMP signalling.

A. Junction of the AS2 helix and the first methylation helix (MH1) of the kinase control domain. Residue positions for AS2 are shaded as in Figs 3 and 7. The N-terminal (MH1) and C-terminal (MH2) methylation helices form a four-helix coiled coil in the Tsr dimer (Kim *et al.*, 1999) (see Fig. 1), with packing interactions mediated by *a-d* heptad repeats (Kim *et al.*, 1999; Alexander and Zhulin, 2007). Left: the heptad packing residues of MH1 are four residues out of phase with those of AS2. Right: helical wheels of the Tsr subunits at the AS2/MH1 junction, showing the alignment of residues in the AS2 helices as they emerge from a stable *x-da* bundle. The *x* positions (not highlighted) are connected by a dashed line. The *a* and *d* positions of the MH1 helices are nearly 180° out of phase, which should destabilize the methylation helices and packing interactions.

B. A modulated dynamics model of HAMP signalling. The model proposes that the *x-da* HAMP bundle is important to both the kinase-activating and kinase-deactivating signalling states because it controls the range of intersubunit motions of the kinase control domain in the Tsr dimer. However, the dynamic states of the *x-da* bundle and methylation helices are oppositely coupled through an out-of-register helical phase relationship; see (A). An unstable *x-da* bundle allows intersubunit interactions of the methylation helices. Conversely, a stable *x-da* bundle destabilizes the methylation helix bundle. The structural interactions between AS2 and MH1 helices are bi-directional. Changes in methylation state modulate stability of the methylation region, which in turn impacts stability of the HAMP bundle. Importantly, this model predicts that attractant stimuli suppress CheA activity by enhancing stability of the HAMP bundle, whereas repellent stimuli should destabilize the bundle. These stimulus-induced changes in HAMP stability could be triggered by small vertical displacements of the transmembrane segments (TM2) adjoining the AS1 helices. The TM2/AS1 connection could act like a control cable to adjust structural tension on the HAMP domain, altering its dynamic properties. See text for additional explanation.

AS2 helices emerge from the HAMP bundle in divergent directions (Hulko *et al.*, 2006), ostensibly in an *x-da* phase arrangement, so their structural interactions with the adjoining MH1 helices might have even more drastic destabilizing consequences (Fig. 8A). Thus, the HAMP and methylation bundles appear to be oppositely coupled through an AS2/MH1 phase clash: stability of one structure should promote instability of the other. We suggest that the interplay between these conformational signals is the essence of HAMP signalling transactions and propose a new mechanistic model of HAMP action based on the dynamic properties of the *x-da* bundle.

A dynamic bundle model of HAMP signalling

There is growing recognition that signalling proteins have dynamic structures that are central to their signalling activities (Smock and Gierasch, 2009). The signalling roles of HAMP domains may be best understood in terms of their dynamic behaviour rather than a few discrete conformational states. The most stable HAMP conformation could be the four-helix *x-da* bundle; the least stable would be a fully denatured bundle. Presumably, HAMP domains have been evolutionarily tuned to operate over some portion of this dynamics range, oscillating between bundle conformations of different stabilities. In our view, HAMP signal output is related to its average bundle stability, reflecting its current conformational space. Stimulus inputs and methylation changes modulate HAMP stability to initiate and terminate signalling responses (Fig. 8B).

The opposed structural coupling between the HAMP and kinase control domains establishes the signalling logic. Chemoreceptors with low-methylation states produce low kinase activity (Li and Weis, 2000; Bornhorst and Falke, 2001; Sourjik and Berg, 2002). Their methylation regions are probably more dynamic than those of highly methylated, CheA-activating receptors (Kim *et al.*, 2002; Starrett and Falke, 2005). Accordingly, stabilization of the HAMP bundle should lower CheA activity; destabilization should increase CheA activity (Fig. 8B). Subsequent methylation or demethylation changes, produced by the sensory adaptation enzymes, would counter these behavioural responses by increasing or decreasing the structural stability of the methylation bundle to offset the HAMP dynamic effects. It follows that attractant stimuli elicit kinase-off responses by stabilizing the HAMP bundle. Because attractants are known to cause an inward piston displacement of the TM2 helices (Falke and Hazelbauer, 2001), stimulus control might involve tension changes in the TM2/AS1 linkage, with no need for the helix rotations implicit in the gearbox model. We suggest that the TM2/AS1 links function as control cables, adjusting structural tension on the HAMP bundle to manipulate its stability (Fig. 8B).

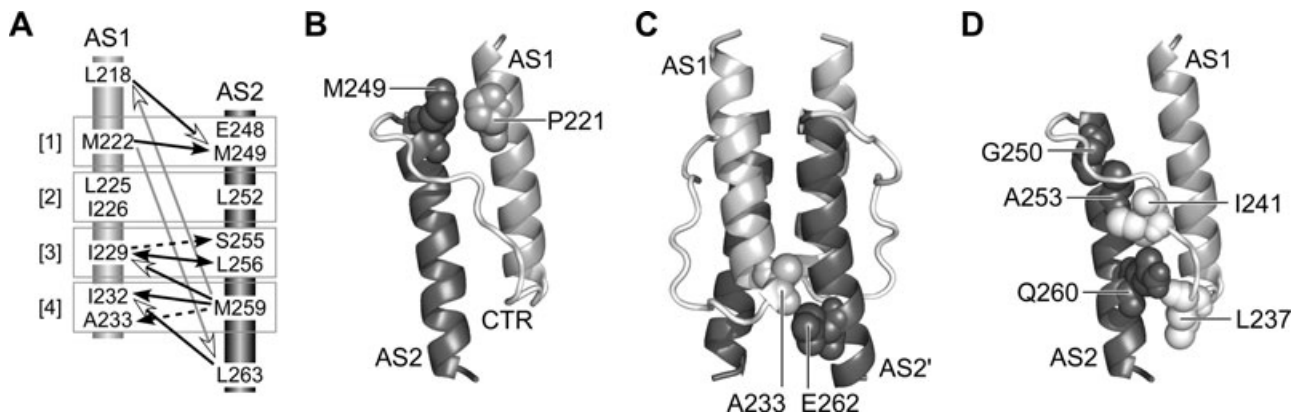


Fig. 9. Structural features of the Tsr-HAMP bundle.

A. Summary of AS1-AS2 suppression effects. Arrows point from the null residue to the suppressor residue. Numbers in brackets identify the packing layers. In the context of the *x-da* bundle structure, suppression effects that should primarily influence the stability of intrasubunit packing are indicated by black lines and arrowheads; effects that should primarily influence the stability of intersubunit packing are indicated by dashed black lines and arrowheads. Inter-layer suppression effects, such as those involving the bundle-capping residues (L218, L263), that could influence both intra- and intersubunit interactions are indicated by open arrowheads: black lines for adjacent layer interactions and grey lines for long-range interactions.

B. Relative positions of P221 and M249 residues in the modelled Tsr-HAMP structure. Only one subunit is shown; the other subunit would be behind these helices.

C. Relative positions of A233 and E262 residues in the modelled Tsr-HAMP structure. The residues abut one another at the subunit interface.

D. Relative positions of AS2 and critical connector residues in the modelled Tsr-HAMP structure. One subunit is shown, as in (B). The side-chains of connector residues L237 and I241 (white, space-filled) project into the AS1-AS2 cleft of the same subunit. Amino acid replacements at AS2 residues G250, A253 and Q260 (dark grey, space-filled) may disrupt HAMP function by displacing the critical connector residues.

Mutational evidence for the dynamic bundle model

The AS1-AS2 conformational suppression effects are more consistent with a dynamic bundle model than a conventional two-state signalling model. In both models, most null lesions should affect function by damaging a signalling structure. The dynamic model predicts that suppressors should restore function by returning HAMP stability to the physiological operating range. In contrast, two-state models predict that some suppressors could restore function by damaging the alternative signalling structure, producing a workable balance between the two compromised states. The structural specificity of the suppression effects argues against this two-state scenario (Fig. 9A). If packing interactions in the wild-type HAMP bundle confer optimal dynamic behaviour, few residue changes outside the null lesion layer would be expected to enhance bundle stability. However, changes within the mutant layer, which is already destabilized, could introduce novel residues that work well in combination with the null replacement, for example, by better filling the altered packing volume or by accommodating water molecules that hydrogen bond to polar groups in the null mutant residue. Thus, null lesions that introduced polar residues at *x* positions (M222Q, I229A/S, L256A/T and M259H) were suppressible by changes that altered the side-chain volume or packing configurations of their major interaction partner in the same layer (M249I/L/V, L256F/I/M, I229F/

L/M and I232M/W respectively) (Fig. 9A). Two-state models predict a wider assortment of suppressors that need not be confined to the vicinity of the original lesion.

The long-range suppression effects (M222Q-L263F; M259T-L218F) involving the bundle-capping residues are interesting exceptions to the general rule of layer-specific suppression, but also understandable in terms of compensatory effects on bundle stability. M222 and M259 are the endmost *x* positions in the bundle. The M222Q and M259T lesions introduce polar groups that should destabilize one end of the bundle, conceivably creating stresses that could be offset by enhanced packing forces at the other end of the bundle. The bundle-capping location is open and better able to accommodate increased side-chain size. Notably, only phenylalanine replacements at L218 and L263 served as long-range suppressors. Phenylalanine is bulkier than leucine and could conceivably create additional bundle-stabilizing forces through stacking interactions.

Bundle stability changes can also account for the few (non-proline) null lesions found at non-critical AS1 and AS2 residues (Fig. 7C). For example, large hydrophobic replacements at P221 disrupted function. In the modelled Tsr-HAMP structure, P221 lies next to M249, a critical *a* residue in AS2 (Fig. 9B). Conceivably, bulky hydrophobics at P221 influence bundle stability through steric and hydrophobic interactions with M249. Similarly, several hydrophobic replacements at E262 (AS2), which borders

on A233, a critical AS1 residue, disrupted function (Fig. 9C). Finally, a few replacements at AS2 residues G250, A253 and Q260, including large hydrophobic, acidic and basic amino acids, disrupted function (Fig. 7C). These null lesions might influence bundle stability through non-specific steric or charge clashes with the connector, which contains several bundle-stabilizing residues (L237 and I241) (Ames *et al.*, 2008). Bulky or charged replacements at AS2 positions that face the connector could weaken those stabilizing connector interactions (Fig. 9D).

Output signals of mutant HAMP domains

HAMP lesions that abrogate chemoreceptor signalling function most likely destabilize the bundle, driving it far enough outside the physiological operating range to prevent effective compensation by the sensory adaptation system. Our current version of the dynamic bundle model does not attempt to define the relationship between HAMP stability and kinase activity outside the normal operating limits. This issue is beyond the scope of the present work, but will be addressed in detail in a follow-up study. However, based on the output patterns of Tsr-HAMP connector mutants, it appears that a very unstable or unstructured HAMP domain can also lock the receptor in a kinase-off mode (Ames *et al.*, 2008). If so, then this kinase-off state is fundamentally different from the attractant-induced signalling state proposed in our model, even though their outputs are the same. This raises a caution flag about drawing mechanistic conclusions from the signal outputs of HAMP mutants in any signalling protein: the relationship between kinase activity and HAMP stability may not be a simple monotonic one.

Generality of the dynamic bundle model

The bundle stability model may also apply to the HAMP domains of signalling proteins other than chemoreceptors. There is evidence for a dynamic or unstructured HAMP state in several other systems (Bordignon *et al.*, 2005; Kishii *et al.*, 2007; Doebber *et al.*, 2008) and the paucity of high-resolution structures implies that HAMP domains could be highly dynamic under physiological conditions. Indeed, the Af1503 HAMP bundle may have been unusually stable because it was examined well below its normal operating temperature (Hulko *et al.*, 2006).

Despite the lack of HAMP structural information in many signalling proteins of interest, it should be possible to test key predictions of the dynamic bundle model by judicious mutant constructions guided by the Tsr-HAMP mutation data. For example: (i) arginine and proline replacements should have opposing dominance effects at x and a/d positions and (ii) the C-terminal (output) end of AS2

should be sensitive to more kinds of amino acid replacements than any other parts of HAMP. These sorts of genetic approaches should help to elucidate structure–function relationships in HAMP domains under *in vivo* operating conditions.

Experimental procedures

Bacterial strains and plasmids

All strains were derivatives of *E. coli* K-12 strain RP437 (Parkinson and Houts, 1982) and contained the following markers relevant to this study: UU1250 [$\Delta aer-1 \Delta tsr-7028 \Delta (tar-tap)5201 \Delta trg-100$] (Ames *et al.*, 2002); UU1535 [$\Delta aer-1 \Delta (tar-cheB)2234 \Delta tsr-7028 \Delta trg-100$] (Bibikov *et al.*, 2004); UU1623 [$\Delta tsr-7028 \Delta tap-3654 \Delta trg-100$] (Ames *et al.*, 2008); UU2377 [$tsr-R69E \Delta aer-1 \Delta (tar-tap)5201 \Delta trg-4543 \Delta recA-SstII/EcoRI$] (Ames *et al.*, 2008); and UU2378 [$tsr-T156K \Delta aer-1 \Delta (tar-tap)5201 \Delta trg-4543 \Delta recA-SstII/EcoRI$] (Ames *et al.*, 2008). Plasmids used in this work were: pKG116, which confers chloramphenicol resistance and has a sodium salicylate-inducible expression/cloning site (Buron-Barral *et al.*, 2006); pPA114, a relative of pKG116 that carries wild-type *tsr* under salicylate control (Ames *et al.*, 2002); pRR48, which confers ampicillin resistance and has an expression/cloning site with a *tac* promoter and ideal (perfectly palindromic) *lac* operator under control of a plasmid-encoded *lacI* repressor, inducible by IPTG (Studdert and Parkinson, 2005); and pRR53, a derivative of pRR48 that carries wild-type *tsr* under IPTG control (Studdert and Parkinson, 2005). Plasmids pKG116 and pPA114 are compatible with plasmids pRR48 and pRR53; both types can stably coexist in the same cell.

Directed mutagenesis

Plasmid mutations were generated by QuikChange mutagenesis, as previously described (Ames *et al.*, 2002). For all-codon mutagenesis, we used oligonucleotide primer pools that were fully degenerate, i.e. with equal frequencies of the four bases A, C, G and T at all three base positions of the targeted codon. Mutations were verified by sequencing the entire *tsr* coding region in the mutant plasmid.

Chemotaxis assays

Host strains carrying Tsr expression plasmids were assessed for chemotactic ability on tryptone soft agar plates (Parkinson, 1976) containing appropriate antibiotics [chloramphenicol ($12.5 \mu\text{g ml}^{-1}$) or ampicillin ($50 \mu\text{g ml}^{-1}$)] and inducer (sodium salicylate or IPTG). Plates were incubated for 7–10 h at 30°C or 32.5°C .

Expression levels of mutant Tsr proteins

The steady-state cellular levels of plasmid-encoded Tsr proteins were assessed in strain UU1535 as described (Ames and Parkinson, 2006).

Protein modelling and structural display

Atomic co-ordinates for the Tsr-HAMP domain were generated from the Af1503-HAMP co-ordinates (PDB ID 2ASW) by the Swiss-Model server (Schwede *et al.*, 2003). Structure images were prepared with MacPyMOL software (<http://www.pymol.org>).

Acknowledgements

Thanks to Tom Alber (U.C. Berkeley) for a most helpful discussion on coiled coils and some useful reality checks. Thanks to Dave Blair (U. Utah) for constructive comments and creative ideas on an earlier version of the manuscript. Thanks to Bob Bourret (U. North Carolina), Joe Falke (U. Colorado), Mike Manson (Texas A and M U), Patricia Mowery (Hobart and William Smith Colleges) and Joachim Schultz (U. Tuebingen) for comments on the manuscript. Thanks to Andrei Lupas (Max Planck Institute – Tuebingen) for thought-provoking discussions. This work was supported by Research Grant GM19559 from the National Institute of General Medical Sciences. The Protein-DNA Core Facility at the University of Utah receives support from National Cancer Institute Grant CA42014 to the Huntsman Cancer Institute.

References

- Alexander, R.P., and Zhulin, I.B. (2007) Evolutionary genomics reveals conserved structural determinants of signaling and adaptation in microbial chemoreceptors. *Proc Natl Acad Sci USA* **104**: 2885–2890.
- Ames, P., and Parkinson, J.S. (2006) Conformational suppression of inter-receptor signaling defects. *Proc Natl Acad Sci USA* **103**: 9292–9297.
- Ames, P., Studdert, C.A., Reiser, R.H., and Parkinson, J.S. (2002) Collaborative signaling by mixed chemoreceptor teams in *Escherichia coli*. *Proc Natl Acad Sci USA* **99**: 7060–7065.
- Ames, P., Zhou, Q., and Parkinson, J.S. (2008) Mutational analysis of the connector segment in the HAMP domain of Tsr, the *Escherichia coli* serine chemoreceptor. *J Bacteriol* **190**: 6676–6685.
- Aravind, L., and Ponting, C.P. (1999) The cytoplasmic helical linker domain of receptor histidine kinase and methyl-accepting proteins is common to many prokaryotic signaling proteins. *FEMS Microbiol Lett* **176**: 111–116.
- Bass, R.B., and Falke, J.J. (1999) The aspartate receptor cytoplasmic domain: *in situ* chemical analysis of structure, mechanism and dynamics. *Structure* **7**: 829–840.
- Bibikov, S.I., Miller, A.C., Gosink, K.K., and Parkinson, J.S. (2004) Methylation-independent aerotaxis mediated by the *Escherichia coli* Aer protein. *J Bacteriol* **186**: 3730–3737.
- Biemann, H.P., and Koshland, D.E., Jr (1994) Aspartate receptors of *Escherichia coli* and *Salmonella typhimurium* bind ligand with negative and half-of-the-sites cooperativity. *Biochemistry* **33**: 629–634.
- Bordignon, E., Klare, J.P., Doebber, M., Wegener, A.A., Martell, S., Engelhard, M., and Steinhoff, H.J. (2005) Structural analysis of a HAMP domain: the linker region of the phototransducer in complex with sensory rhodopsin II. *J Biol Chem* **280**: 38767–38775.
- Bornhorst, J.A., and Falke, J.J. (2001) Evidence that both ligand binding and covalent adaptation drive a two-state equilibrium in the aspartate receptor signaling complex. *J Gen Physiol* **118**: 693–710.
- Brown, J.H., Cohen, C., and Parry, D.A. (1996) Heptad breaks in alpha-helical coiled coils: stutters and stammers. *Proteins* **26**: 134–145.
- Buron-Barral, M., Gosink, K.K., and Parkinson, J.S. (2006) Loss- and gain-of-function mutations in the F1-HAMP region of the *Escherichia coli* aerotaxis transducer Aer. *J Bacteriol* **188**: 3477–3486.
- Butler, S.L., and Falke, J.J. (1998) Cysteine and disulfide scanning reveals two amphiphilic helices in the linker region of the aspartate chemoreceptor. *Biochemistry* **37**: 10746–10756.
- Doebber, M., Bordignon, E., Klare, J.P., Holterhues, J., Martell, S., Mennes, N., *et al.* (2008) Salt-driven equilibrium between two conformations in the HAMP domain from *Natronomonas pharaonis*: the language of signal transfer? *J Biol Chem* **283**: 28691–28701.
- Falke, J.J., and Hazelbauer, G.L. (2001) Transmembrane signaling in bacterial chemoreceptors. *Trends Biochem Sci* **26**: 257–265.
- Hazelbauer, G.L., Falke, J.J., and Parkinson, J.S. (2008) Bacterial chemoreceptors: high-performance signaling in networked arrays. *Trends Biochem Sci* **33**: 9–19.
- Hulko, M., Berndt, F., Gruber, M., Linder, J.U., Truffault, V., Schultz, A., *et al.* (2006) The HAMP domain structure implies helix rotation in transmembrane signaling. *Cell* **126**: 929–940.
- Inoue, K., Sasaki, J., Spudich, J.L., and Terazima, M. (2008) Signal transmission through the HtrII transducer alters the interaction of two alpha-helices in the HAMP domain. *J Mol Biol* **376**: 963–970.
- Kim, K.K., Yokota, H., and Kim, S.H. (1999) Four-helical-bundle structure of the cytoplasmic domain of a serine chemotaxis receptor. *Nature* **400**: 787–792.
- Kim, S.H., Wang, W., and Kim, K.K. (2002) Dynamic and clustering model of bacterial chemotaxis receptors: structural basis for signaling and high sensitivity. *Proc Natl Acad Sci USA* **99**: 11611–11615.
- Kishii, R., Falzon, L., Yoshida, T., Kobayashi, H., and Inouye, M. (2007) Structural and functional studies of the HAMP domain of EnvZ, an osmosensing transmembrane histidine kinase in *Escherichia coli*. *J Biol Chem* **282**: 26401–26408.
- Lai, W.C., Beel, B.D., and Hazelbauer, G.L. (2006) Adaptational modification and ligand occupancy have opposite effects on positioning of the transmembrane signalling helix of a chemoreceptor. *Mol Microbiol* **61**: 1081–1090.
- Lee, L., Mizuno, T., and Imae, Y. (1988) Thermosensing properties of *Escherichia coli* tsr mutants defective in serine chemoreception. *J Bacteriol* **170**: 4769–4774.
- Li, G., and Weis, R.M. (2000) Covalent modification regulates ligand binding to receptor complexes in the chemosensory system of *Escherichia coli*. *Cell* **100**: 357–365.
- Lin, L.N., Li, J., Brandts, J.F., and Weis, R.M. (1994) The serine receptor of bacterial chemotaxis exhibits half-site saturation for serine binding. *Biochemistry* **33**: 6564–6570.
- Lupas, A. (1996) Coiled coils: new structures and new functions. *Trends Biochem Sci* **21**: 375–382.

- Milburn, M.V., Prive, G.G., Milligan, D.L., Scott, W.G., Yeh, J., Jancarik J., *et al.* (1991) Three-dimensional structures of the ligand-binding domain of the bacterial aspartate receptor with and without a ligand. *Science* **254**: 1342–1347.
- Milligan, D.L., and Koshland, D.E., Jr (1988) Site-directed cross-linking. Establishing the dimeric structure of the aspartate receptor of bacterial chemotaxis. *J Biol Chem* **263**: 6268–6275.
- Mowery, P., Ostler, J.B., and Parkinson, J.S. (2008) Different signaling roles of two conserved residues in the cytoplasmic hairpin tip of Tsr, the *Escherichia coli* serine chemoreceptor. *J Bacteriol* **190**: 8065–8074.
- Park, S.Y., Borbat, P.P., Gonzalez-Bonet, G., Bhatnagar, J., Pollard, A.M., Freed, J.H., *et al.* (2006) Reconstruction of the chemotaxis receptor-kinase assembly. *Nat Struct Mol Biol* **13**: 400–407.
- Parkinson, J.S. (1976) *cheA*, *cheB*, and *cheC* genes of *Escherichia coli* and their role in chemotaxis. *J Bacteriol* **126**: 758–770.
- Parkinson, J.S., and Houts, S.E. (1982) Isolation and behavior of *Escherichia coli* deletion mutants lacking chemotaxis functions. *J Bacteriol* **151**: 106–113.
- Pollard, A.M., Bilwes, A.M., and Crane, B.R. (2009) The structure of a soluble chemoreceptor suggests a mechanism for propagating conformational signals. *Biochemistry* **48**: 1936–1944.
- Schwede, T., Kopp, J., Guex, N., and Peitsch, M.C. (2003) SWISS-MODEL: an automated protein homology-modeling server. *Nucleic Acids Res* **31**: 3381–3385.
- Smock, R.G., and Gierasch, L.M. (2009) Sending signals dynamically. *Science* **324**: 198–203.
- Sourjik, V., and Berg, H.C. (2002) Receptor sensitivity in bacterial chemotaxis. *Proc Natl Acad Sci USA* **99**: 123–127.
- Starrett, D.J., and Falke, J.J. (2005) Adaptation mechanism of the aspartate receptor: electrostatics of the adaptation subdomain play a key role in modulating kinase activity. *Biochemistry* **44**: 1550–1560.
- Studdert, C.A., and Parkinson, J.S. (2004) Crosslinking snapshots of bacterial chemoreceptor squads. *Proc Natl Acad Sci USA* **101**: 2117–2122.
- Studdert, C.A., and Parkinson, J.S. (2005) Insights into the organization and dynamics of bacterial chemoreceptor clusters through *in vivo* crosslinking studies. *Proc Natl Acad Sci USA* **102**: 15623–15628.
- Swain, K.E., and Falke, J.J. (2007) Structure of the conserved HAMP domain in an intact, membrane-bound chemoreceptor: a disulfide mapping study. *Biochemistry* **46**: 13684–13695.
- Watts, K.J., Johnson, M.S., and Taylor, B.L. (2008) Structure-function relationships in the HAMP and proximal signaling domains of the aerotaxis receptor Aer. *J Bacteriol* **190**: 2118–2127.
- Williams, S.B., and Stewart, V. (1999) Functional similarities among two-component sensors and methyl-accepting chemotaxis proteins suggest a role for linker region amphipathic helices in transmembrane signal transduction. *Mol Microbiol* **33**: 1093–1102.
- Yang, Y., Park, H., and Inouye, M. (1993) Ligand binding induces an asymmetrical transmembrane signal through a receptor dimer. *J Mol Biol* **232**: 493–498.

Supporting information

Additional supporting information may be found in the online version of this article.

Please note: Wiley-Blackwell are not responsible for the content or functionality of any supporting materials supplied by the authors. Any queries (other than missing material) should be directed to the corresponding author for the article.

Table S1

residue	mutant amino acid	protein level relative to wild-type ^a	dominance test ^b		mixed trimer test in UU1623 rescue ^d	
			UU2377 (R69E)	UU2378 (T156K)	jamming ^c	rescue ^d
K215	P	0.8	+	+	no	no
S217	P	1.0	+	+	no	R1
L218	E	1.4	+	+	no	no
	K	1.1	+	+	no	(R2)
	N	1.3	+	+	no	R2
	P	0.9	0	0	E1	no
	R	1.1	+	+	no	(R2)
P221	F	0.9	+	+	E2	no
	I	0.6	+	+	no	R1
	L	0.7	+	+	no	R1
	W	0.7	+	+	no	R2
M222	D	0.9	+	+	no	no
	E	1.0	+	+	no	no
	N	1.3	+	+	no	no
	P	1.3	+	+	no	no
	Q	1.4	+	+	E1	no
	R	1.1	0	0	E1	no
L225	C	1.5	+	+	no	R2
	D	1.5	+	+	no	no
	G	1.0	+	+	no	(R2)
	K	1.0	+	+	no	no
	P	0.9	0	0	no	no
	Q	1.9	+	+	no	R2
	R	1.4	+	+	no	(R1)
	S	2.0	+	+	no	R2
I226	P	0.9	+	+	no	no
D227	M	0.2	ND	ND	no	no
	P	0.1	ND	ND	no	no
S228	P	0.7	+	+	no	R2
I229	A	1.0	+	+	E1	(R2)
	D	1.0	0	0	no	no
	E	0.6	+	+	no	no
	P	0.9	+	+	no	no
	R	1.1	0	0	no	no
	S	0.8	+	+	E1	R2
I232	D	2.1	0	0	no	no

	E	1.1	+	+	no	no
	G	1.6	+	+	no	no
	H	1.4	+	+	no	(R2)
	K	1.6	+	+	no	no
	N	0.8	+	+	no	no
	P	0.9	+	+	E1	no
	R	2.0	+	+	no	no
	S	1.6	+	+	no	(R2)
A233	C	0.9	+	+	no	R2
	F	0.7	+	+	no	R2
	I	0.9	+	+	no	R2
	L	0.9	+	+	E2	no
	N	0.7	+	+	E1	no
	P	1.0	+	+	no	R1
	V	0.7	+	+	E1	no
E248	G	0.8	+	+	no	R2
	H	1.1	+	+	no	R2
	I	0.9	+	+	no	R1
	K	1.1	+	+	E1	no
	L	1.0	+	+	E2	no
	M	0.8	+	+	E2	no
	N	0.8	+	+	no	R1
	P	0.8	+	+	no	R2
	Q	1.0	+	+	no	R2
	R	1.4	+	+	E1	no
	T	1.1	+	+	no	R2
	V	1.1	+	+	no	R1
M249	D	0.6	+	+	no	no
	E	0.7	+	+	no	no
	G	0.8	+	+	no	(R2)
	K	1.0	+	+	no	no
	Q	1.3	+	+	no	(R2)
	R	1.0	+	+	no	no
G250	P	1.0	+	+	E1	no
	W	0.8	+	+	no	R3
Q251	P	1.1	+	+	no	R1
L252	E	0.7	0	0	no	no
	H	0.5	+	+	no	no
	K	1.5	0	0	E1	no
	N	0.9	0	0	no	no

Supporting Information - Zhou *et al.*

	P	0.6	+	+	no	no
	R	0.9	0	0	no	no
	S	1.0	+	+	no	no
A253	D	1.0	+	+	no	no
	I	0.6	+	+	no	no
	K	0.8	+	+	no	(R1)
	P	1.0	+	+	E1	no
	R	1.1	+	+	no	R1
E254	P	0.8	+	+	no	no
S255	L	1.0	+	+	E1	R1
	P	1.2	+	+	no	(R2)
L256	A	0.7	+	+	E1	(R2)
	E	1.0	0	0	E3	no
	G	2.0	+	+	E3	no
	K	1.0	0	0	no	no
	N	1.9	0	0	no	no
	P	1.7	0	0	E3	no
	Q	0.7	0	0	E3	no
	R	0.7	0	0	E3	no
	S	0.6	+	+	E3	no
	T	0.6	+	+	E1	(R2)
	Y	1.0	+	+	E2	(R2)
R257	P	0.9	0	0	E1	no
H258	P	1.2	0	0	E1	no
M259	D	1.1	0	0	no	no
	E	1.0	0	0	no	no
	F	2.6	+	+	E1	(R2)
	H	1.1	+	+	E3	no
	I	0.8	0	0	E3	no
	K	1.8	+	+	E3	no
	P	1.1	+	+	E1	no
	Q	1.1	+	+	no	(R2)
	R	0.8	0	0	E3	no
	T	0.8	+	+	E3	(R2)
	V	0.9	0	0	E3	no
Q260	D	0.6	+	+	E1	no
	F	0.8	±	+	no	R1
	P	0.7	0	0	E1	no
G261	P	0.6	0	0	E1	no
E262	I	0.8	±	+	E2	R2

	L	1.0	0	0	E2	R2
	P	0.8	+	+	E1	R2
L263	A	0.7	+	+	E1	(R2)
	C	0.6	+	+	E1	(R2)
	E	0.9	0	0	E3	no
	G	1.0	+	+	E3	no
	N	0.9	+	+	no	no
	P	0.8	0	0	E3	no
	R	0.8	0	0	E3	no
	S	0.7	+	+	E3	no
	T	0.8	+	+	E1	(R2)
	Y	0.8	+	+	no	R2
M264	P	0.9	0	0	E1	no
	Y	0.0	ND	ND	no	no
R265	P	1.0	+	+	E1	no

^a Values are rounded to one decimal place.

^b Results of complementation tests between plasmid-borne *tsr*-HAMP null mutations and strains with a recessive *tsr* serine-binding lesion (R69E or T156K); 0 = no complementation (Tsr^-); + = complementation (Tsr^+); ND = not done due to low expression level of mutant protein.

^c Results of Tar function tests in UU1623 ($\Delta tsr tar^+$) cells carrying plasmid-borne *tsr*-HAMP null mutations. Tar-jamming effects, if any, were classified from least to most severe on a scale (E1-E3) based on the level of Tsr^* expression needed for the effect (Ames *et al.*, 2002).

^d Results of Tsr function tests in UU1623 ($\Delta tsr tar^+$) cells carrying plasmid-borne *tsr*-HAMP null mutations. Rescue of Tsr function, if any, was classified from least to most effective on a scale (R1-R3) based on the level of Tsr^* expression needed for the effect (Ames *et al.*, 2002). Rescue effects shown in parentheses occurred at 30°C, but not at 32.5°C.